

Spectral Distortion of the CMB by the Cumulative CO Emission from Galaxies throughout Cosmic History

Natalie Mashian^{1*}, Abraham Loeb^{1†}, Amiel Sternberg^{2‡}

¹*Harvard-Smithsonian Center for Astrophysics, 60 Garden Street, Cambridge, MA 02138, USA*

²*The Raymond and Beverly Sackler School of Physics and Astronomy, Tel Aviv University, Tel Aviv 69978, Israel*

18 February 2016

ABSTRACT

We show that the cumulative CO emission from galaxies throughout cosmic history distorts the spectrum of the cosmic microwave background (CMB) at a level that is well above the detection limit of future instruments, such as the Primordial Inflation Explorer (PIXIE). The modeled CO signal has a prominent bump in the frequency interval 100–200 GHz, with a characteristic peak intensity of $\sim 2 \times 10^{-23} \text{ W m}^{-2} \text{ Hz}^{-1} \text{ sr}^{-1}$. Most of the CO foreground originates from modest redshifts, $z \sim 2$ –5, and needs to be efficiently removed for more subtle distortions from the earlier universe to be detected.

Key words: cosmology: cosmic background radiation – cosmology: theory, early universe – galaxies: intergalactic medium

1 INTRODUCTION

Since the measurements by COBE/Far Infrared Absolute Spectrophotometer (FIRAS), the average cosmic microwave background spectrum (CMB) spectrum is known to be extremely close to a perfect blackbody with a temperature $T_0 = 2.726 \pm 0.001 \text{ K}$ and no detected global spectral distortions to date (Mather et al. 1994; Fixsen et al. 1996; Fixsen 2009). However, the standard model of cosmology predicts tiny deviations from the Planckian spectrum due to cosmological processes which heat, cool, scatter, and create CMB photons throughout the history of the Universe (Sunyaev & Zeldovich 1969; Zeldovich & Sunyaev 1969; Sunyaev & Zeldovich 1970; Illarionov & Sunyaev 1975a,b; Danese & de Zotti 1982; Burigana, Danese, & de Zotti 1991; Hu & Silk 1993; Burigana & Salvaterra 2003; Chluba, Khatri, & Sunyaev 2012; Sunyaev & Khatri 2013). While at redshifts $z \gtrsim 2 \times 10^6$, the thermalization process (mediated by the combined action of double Compton emission, Bremsstrahlung and Compton scattering) is rapid enough to efficiently erase any distortion to unobservable levels, at lower redshifts, the CMB spectrum becomes vulnerable and spectral distortions that form are “locked in” and can thus be theoretically observed today (Chluba & Sunyaev 2012; Chluba 2014; Chluba, Hamann, & Patil 2015).

In connection with early energy release, two types of CMB distortions are traditionally distinguished:

chemical potential μ - and Compton y - distortions (Sunyaev & Zeldovich 1969, 1970; Illarionov & Sunyaev 1975a,b). In the regime $2 \times 10^6 \lesssim z \lesssim 3 \times 10^5$, the efficiency of double Compton and Bremsstrahlung processes in controlling the number of CMB photons gradually reduces while photons are still efficiently redistributed in energy by the Compton process. In this case, where thermalization stops being complete, electrons and photons are in kinetic equilibrium with respect to Compton scattering, and any energy injection produces a chemical potential characterized by $\mu(\nu)$. At lower redshifts, $z \lesssim 10^4$, up-scattering of photons by electrons also becomes inefficient and photons diffuse only little in energy, creating a y -type distortion $y(\nu)$ which is an early-universe analogue of the thermal Sunyaev-Zeldovich effect. Both types of distortions are tightly constrained by COBE/FIRAS measurements, with upper limits of $|\mu| < 9 \times 10^{-5}$ and $|y| < 1.5 \times 10^{-5}$ at 95% confidence (Fixsen et al. 1996).

The amplitude of these signals, predicted within the standard cosmological paradigm, is expected to fall below the bounds set by COBE-FIRAS measurements. The average amplitude of the y -parameter, due to the large-scale structure and the reionization epoch, is expected to be $y \simeq 10^{-7}$ – 10^{-6} , with the most recent computations predicting $y \simeq 2 \times 10^{-6}$ (Hu, Scott, & Silk 1994a; Refregier et al. 2000; Oh, Cooray, & Kamionkowski 2003; Hill et al. 2015). The μ -distortion signal is expected to be even weaker, with the damping of small-scale acoustic modes giving rise to $\mu \simeq 2 \times 10^{-8}$ in the standard slow-roll inflation scenario (Daly 1991; Hu, Scott, & Silk 1994b; Chluba, Khatri, & Sunyaev 2012). Although these distortions are small, significant progress in technology in the last two decades promises

* nmashian@physics.harvard.edu

† aloeb@cfa.harvard.edu

‡ amiel@wise.tau.ac.il

to detect these spectral distortions. Experimental concepts, like the Primordial Inflation Explorer (PIXIE; Kogut et al. 2011a) and Polarized Radiation Imaging and Spectroscopy Mission (PRISM; André et al. 2014), could possibly improve the absolute spectral sensitivity limits of COBE/FIRAS by 2-3 orders of magnitude and detect the aforementioned signals at the 5σ level, providing measurements at sensitivities $\mu = 5 \times 10^{-8}$ for a chemical potential distortion and $y = 10^{-8}$ for a Compton distortion (Fixsen & Mather 2002; Kogut et al. 2011a; Chluba 2013; Chluba & Jeong 2014).

However, it is not yet clear what the foreground limitations to measuring these primordial spectral distortions will be. When considering the large angular scales of interest to PIXIE, focus has been geared towards the foreground subtraction of polarized emission from the Milky Way’s interstellar medium (ISM) which is dominated by synchrotron radiation from cosmic ray electrons accelerated in the Galactic magnetic field, and thermal emission from dust grains. Kogut et al. (2011b) claim that the CMB emission can be distinguished from Galactic foregrounds based on their different frequency spectra, as long as the number of independent frequency channels equals or exceeds the number of free parameters to be derived from a multi-frequency fit.

But in addition to these Galactic foregrounds, there is another contaminant which has been primarily neglected in the literature, and that is the diffuse background of CO emission lines from external galaxies. Until recently, Righi, Hernández-Montegudo, & Sunyaev (2008) provided the only estimate of this redshift-integrated CO emission signal. Assuming star formation is driven by major mergers, they calculated the resulting star-formation rate (SFR) and then converted it to a CO luminosity, L_{CO} , using the measured ratio of L_{CO} to SFR in M82, a low-redshift starburst galaxy. The CO background they found, integrated over all redshifts, is expected to contribute $\sim 1 \mu\text{K}$ at $\nu \gtrsim 100$ GHz with an almost flat spectrum. De Zotti et al. (2015) also include estimates of the background contributed by CO lines from star-forming galaxies when they consider the Galactic and extragalactic foreground intensity compared with the CMB spectra. Using the $L_{\text{IR}}-L_{CO}$ relations presented in Greve et al. (2014) for the CO rotational ladder from $J = 1 \rightarrow 0$ to $J = 5 \rightarrow 4$, they find that the CO signal is substantially higher than the PIXIE sensitivity, with the CO(4-3) line alone contributing $\sim 3 \times 10^{-24} \text{ erg s}^{-1} \text{ cm}^{-2} \text{ sr}^{-1}$ at sub-mm wavelengths.

In this paper, we apply the formalism and machinery presented in Mashian, Sternberg, & Loeb (2015) to predict the total CO emission signal generated by a population of star-forming halos with masses $M \geq 10^{10} M_{\odot}$ from the present-day, to redshifts as early as $z \sim 15$. Our comprehensive approach is based on large-velocity gradient (LVG) modeling, a radiative transfer modeling technique that produces the full CO spectral line energy distribution (SLED) for a specified set of parameters characterizing the emitting source. By linking these parameters to the global properties of the host halos, we calculate the CO line intensities emitted by a halo of mass M at redshift z , and then further integrate these CO luminosities over the range of halo masses hosting CO-luminous galaxies to derive the average surface brightness of each rotational line. We find that over a range of frequencies (30-300 GHz) spanned by a PIXIE-like mission, the signal strength of this diffuse background is

1-3 orders of magnitude larger than the spectral distortion limits PIXIE aims to provide. The CO foreground must be removed in order for the more subtle distortion signals from the earlier universe to be detected.

This Letter is organized as follows. Section 2 provides a brief overview of the formalism and key ingredients of our CO-signal modeling technique. Section 3 presents the results and Section 4 summarizes the main conclusions. We adopt a flat, Λ CDM cosmology with $\Omega_m = 0.3$, $\Omega_{\Lambda} = 0.7$, $\Omega_b = 0.045$, $H_0 = 70 \text{ km s}^{-1} \text{ Mpc}^{-1}$ (i.e. $h = 0.7$), $\sigma_8 = 0.82$, and $n_s = 0.95$, consistent with the most recent measurements from Planck (Planck Collaboration et al. 2015).

2 THE FORMALISM

In Mashian, Sternberg, & Loeb (2015), we developed a novel approach to estimating the line intensity of any CO rotational transition emitted by a host halo with mass M at redshift z in the early universe, $z \geq 4$. Here, we briefly outline the model far enough to calculate the quantities relevant for the present work and refer the reader to our previous paper for further details.

In our formalism, the average specific intensity of a given CO line with rest-frame frequency ν_J emitted by gas at redshift z_J is,

$$I_{\nu_{obs}} = \frac{c}{4\pi} \frac{1}{\nu_J H(z_J)} \int_{M_{min,CO}}^{\infty} dM \frac{dn}{dM}(M, z_J) L(M, z_J) \quad (1)$$

where $H(z)$ is the Hubble parameter, dn/dM is the Sheth-Tormen halo mass function (Sheth & Tormen 1999) and $M_{min,CO}$ is the minimum host halo mass for CO-luminous galaxies. To determine the specific luminosity of the line, $L(M, z_J)$, we employ LVG modeling, a method of radiative transfer in which the excitation and opacity of CO lines are determined by the kinetic temperature T_{kin} , velocity gradient dv/dr , gas density n , CO-to-H₂ abundance ratio χ_{CO} , and the CO column density N_{CO} of the emitting source. A background radiation term with temperature, $T_{CMB} = T_0(1+z)$, is included in the LVG calculations; the increasing CMB temperature with z is expected to depress the CO line luminosity at higher redshifts. Adopting the escape probability formalism (Castor 1970; Goldreich & Kwan 1974) for a spherical cloud undergoing uniform collapse and assuming that each emitting source consists of a large number of these unresolved collapsing clouds, the emergent LVG-modeled intensity of an emission line can be expressed as

$$I_J = \frac{h\nu_J}{4\pi} A_J x_J \beta_J (\tau_J) \chi_{CO} N_{H_2} \quad (2)$$

where x_J is the population fraction in the J^{th} level, A_J is the Einstein radiative coefficient, N_{H_2} is the beam-averaged H₂ column density, and $\beta_J = (1 - e^{-\tau_J})/\tau_J$ is the photon-escape probability. To carry out these computations, we use the Mark & Sternberg LVG radiative transfer code described in Davies et al. (2012).

We showed previously that the LVG parameters, $\{T_{kin}, n_{H_2}, dv/dr, \chi_{CO}, \text{ and } N_{H_2}\}$, which drive the physics of CO transitions and ultimately dictate both the shape and amplitude of the resulting CO SLED, can be linked to the emitting galaxy’s global star formation rate, SFR , and the star formation rate surface density, Σ_{SFR} . The analytic expressions for these quantities can be found in Section 2.3

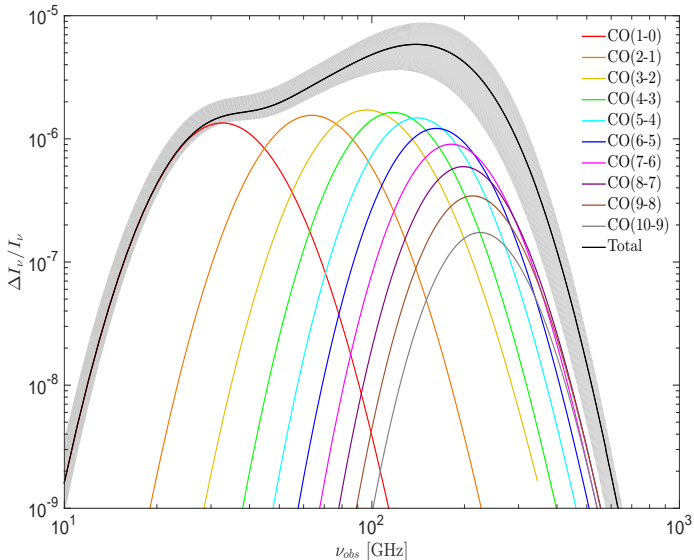


Figure 1. The relative CMB spectral distortions due to CO emission from star-forming galaxies at redshifts as high as $z \sim 15$ to the present. The contribution of each spectral line, from $J = 1 \rightarrow 0$ to $J = 10 \rightarrow 9$ is shown, along with the summed signal (black curve). The shaded area corresponds to the 1σ confidence region for the total predicted signal.

of Mashian, Sternberg, & Loeb (2015), and will not be re-derived here. The final ingredient in our model is thus a $SFR - M$ relation that allows us to express these LVG parameters solely as functions of the global properties of the host halo, i.e. the halo mass M and redshift z .

For high redshifts, $z \geq 4$, we adopt the average $SFR - M$ relation derived in Mashian, Oesch, & Loeb (2016) via abundance-matching. Assuming each dark-matter halo hosts a single galaxy, they mapped the shape of the observed ultraviolet luminosity functions (UV LFs) at $z \sim 4-8$ to that of the halo mass function at the respective redshifts and found that the $SFR - M$ scaling law is roughly constant across this redshift range (within 0.2 dex). This average relation, which faithfully reproduces the observed $z \sim 9 - 10$ LFs, is therefore employed in our calculations for all redshifts greater than 4. For $z < 4$, we rely on the results of Behroozi, Wechsler, & Conroy (2013a,b) which empirically quantified the stellar mass history of dark matter halos, using a comprehensive compilation of observational data along with simulated halo merger trees to constrain a parameterized stellar mass-halo mass relation.

3 RESULTS

In Figure 1, we present our predictions of the contribution of each spectral line to the cumulative CO background from star-forming galaxies at redshifts as high as $z \sim 15$ to the present. The low- J CO lines peak at frequencies corresponding to an emission redshift of $z \sim 2$. This emission is dominated by star-forming halos with masses $10^{11}-10^{12} M_{\odot}$, hosting molecular clouds that are characterized by a gas kinetic temperature $T_{\text{kin}} \sim 40$ K and H_2 number densities $n_{\text{H}_2} \sim$

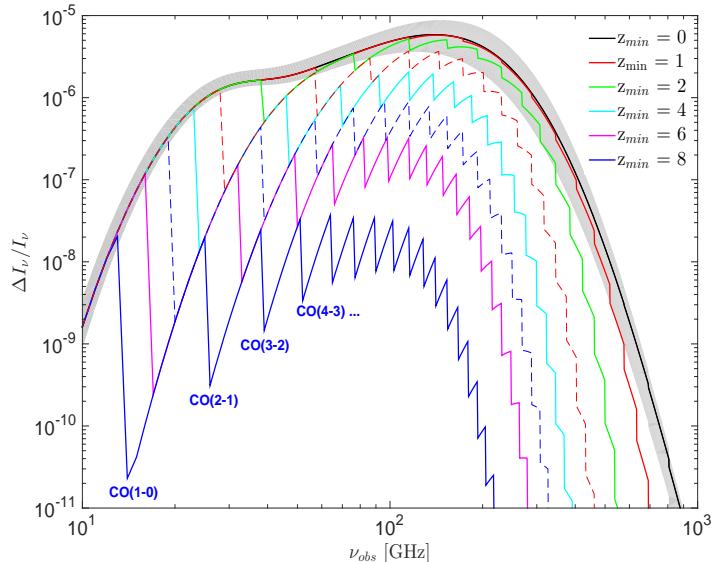


Figure 2. The relative CMB spectral distortions due to the cumulative CO foreground emission from galaxies at redshifts between $z = z_{\text{min}}$ and $z = 15$.

$100 - 1000 \text{ cm}^{-3}$. The higher- J ($J > 5$) CO signal is dominated by emission from $10^{11}-10^{12} M_{\odot}$ host halos residing at $z \gtrsim 4$; in the star-forming galaxies at these high redshifts, the physical conditions in the emitting molecular clouds are extreme enough to thermalize the higher-order CO transitions, with gas kinetic temperatures of ~ 60 K and number densities of order 10^4 cm^{-3} . Integrating over the population of CO luminous halos between redshifts $0 \leq z \leq 15$, we find that the total emission (black curve) predicted by our LVG-based model is not completely spectrally smooth, but rather has a prominent bump in the frequency interval $\sim 100 - 200$ GHz with a characteristic peak intensity of $\sim 2 \times 10^{-23} \text{ W m}^{-2} \text{ Hz}^{-1} \text{ sr}^{-1}$, i.e. $\Delta I_{\nu}/I_{\nu} \simeq (5 \pm 2) \times 10^{-6}$. This is the frequency range within which the most prominent redshifted CO line emissions, originating from sources at redshifts $z \sim 2 - 5$, fall and accumulate to form the peak in the cumulative signal depicted in Figure 1. The total CO intensity is $\sim 0.01\%$ of the far-infrared background intensity computed in Fixsen et al. (1998) and Lutz (2014), where the former computes a total $125-2000 \mu\text{m}$ background of $\sim 14 \text{ nW m}^{-2} \text{ sr}^{-1}$ and the latter computes a total $8-1000 \mu\text{m}$ background of $\sim 27 \text{ nW m}^{-2} \text{ sr}^{-1}$. The uncertainty in our estimates of the CO signal, represented by the shaded regions in Figures 1-3, primarily stems from the uncertainty in the average $SFR - M$ relations we adopt to express the LVG parameters as functions of the global properties of the host halos.

In the case where we assume that local sources of CO emission can be identified and subtracted from observations, we find that the predicted foreground signal not only drops in magnitude as expected, but the shape of the CO spectrum is modified as well. These results are clearly demonstrated in Figure 2, where each curve is computed by integrating the CO intensity emitted by galaxies from some minimum redshift, z_{min} , out to redshift $z \simeq 15$. Starting off with $z_{\text{min}} = 0$, which corresponds to the original results shown in Fig-

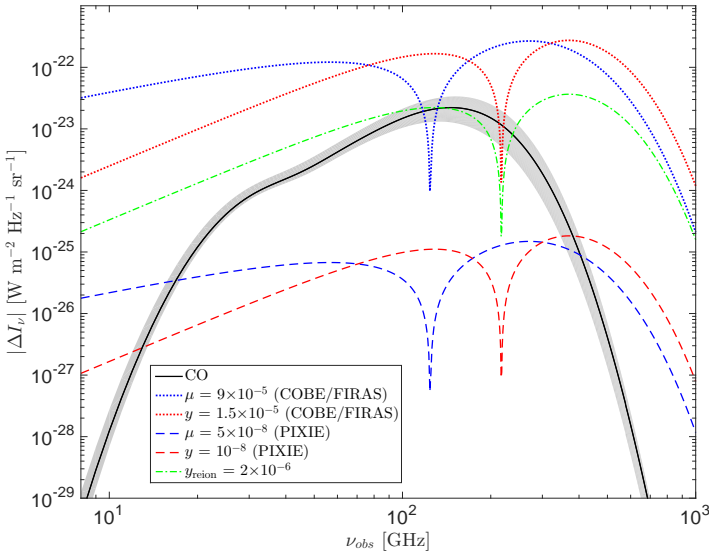


Figure 3. μ -type and y -type spectral distortions corresponding to the current COBE/FIRAS limits (2σ ; dotted curves) and the anticipated PIXIE sensitivity limits (5σ ; dashed curves). The absolute value of the difference in intensity from the blackbody spectrum is shown where ΔI_ν^μ and ΔI_ν^y are given by equations (3) and (4), respectively. The green dash-dot curve represents the y -type distortions due to reionization and structure formation in the late Universe, $z \lesssim 10 - 20$. The cusp in each curve signifies the transition from a negative distortion to a positive distortion, with a zero point/crossing frequency of $\nu = 124$ and 217 GHz for μ - and y -type distortions, respectively.

ure 1 where emission from local sources is included in the calculations (black curve), we vary the minimum redshift to values as high as $z_{\min} = 8$. We find that excluding the emission from the population of lower redshift sources results in a sawtooth modulation of the cumulative CO spectrum, with the modulation appearing at the observed frequencies, $\nu_{\text{obs}} = \nu_J / (1 + z_{\min})$, at which the contribution from a given CO transition, $J \rightarrow J-1$, drops out. For example, in the case where emission sources at redshifts $z < 4$ can be subtracted and thus no longer contribute to the CO foreground (blue curve), the total CO signal strength plummets at $\nu_{\text{obs}} \simeq 23$ GHz when the CO(1-0) line contribution disappears, and then again at $\nu_{\text{obs}} \simeq 46$ GHz when the CO(2-1) contribution dies out; this pattern continues out to $\nu_{\text{obs}} \simeq 922$ GHz, at which point the redshifted CO($J = 40 \rightarrow 39$) line vanishes and no trace of the CO signal emitted by the galaxy population at $z \geq 4$ is left. This sawtooth-shaped form of the resulting CO spectrum highlights both the discrete nature of CO rotational transitions at frequencies, $\nu_J = J\nu_{\text{CO}(1-0)}$, with $\nu_{\text{CO}(1-0)} = 115.3$ GHz and $J = 1, 2, \dots, 40$, as well as the significant contribution by modest redshift sources to the overall CO foreground signal.

Assuming that the more local emission sources are not individually subtracted, the intensity of the predicted CO background is at least 2-100 times weaker than the current COBE/FIRAS upper limits, $\Delta I_\nu / I_\nu \lesssim 10^{-5} - 10^{-4}$. Therefore, although this foreground is expected to peak in the range of frequencies spanned by COBE/FIRAS, the signal has eluded detection to date. However, as depicted in Figure

3, the total emission one expects from the CO background lies 1-3 orders of magnitude above the PIXIE sensitivity to μ - and y -type distortions in the 30-300 GHz frequency range. These spectral distortions take the form

$$\Delta I_\nu^\mu = \frac{2h\nu^3}{c^2} \times \mu \frac{e^x}{(e^x - 1)^2} \left(\frac{x}{2.19} - 1 \right) \quad (3)$$

and

$$\Delta I_\nu^y = \frac{2h\nu^3}{c^2} \times y \frac{xe^x}{(e^x - 1)^2} \left[x \left(\frac{e^x + 1}{e^x - 1} \right) - 4 \right] \quad (4)$$

where $x = h\nu / (k_B T)$ is the dimensionless frequency, h is Planck's constant, k_B is Boltzmann's constant, and T is the CMB temperature. The full exploitation of PIXIE's potential to measure μ - and y -type spectral distortions of $\mu = 5 \times 10^{-8}$ and $y = 10^{-8}$ at the 5σ level therefore requires a highly refined foreground subtraction, which is further complicated by the fact that the CO signal is not completely spectrally smooth. At higher frequencies, $\nu \gtrsim 400$ GHz, the foreground CO emission grows exponentially weak, $\Delta I_\nu^{\text{CO}} \ll \Delta I_\nu^\mu, \Delta I_\nu^y$, and ceases to pose as a prominent limiting factor in obtaining accurate spectral distortion measurements. The y distortion from reionization and structure formation ($z \lesssim 10 - 20$; green curve), has a relatively large amplitude, $|y| \sim 2 \times 10^{-6}$, comparable to the predicted cumulative CO signal, and is expected to be visible even without more detailed modeling.

4 DISCUSSION

We apply an LVG-based modeling approach to predict the cumulative CO emission signal generated by star-forming galaxies throughout cosmic history. The relative CMB distortion due to this CO foreground is not spectrally smooth, but rather peaks in the frequency range $\nu \sim 100 - 200$ GHz with an amplitude of $\Delta I_\nu / I_\nu \simeq 5 \times 10^{-6}$. Exploring cases where nearby sources of CO emission can be identified and subtracted from observations, we find that the dominant contributors to the CO signal originate from star-forming halos with masses $M \sim 10^{11} - 10^{12} M_\odot$ at modest redshifts of $z \sim 2 - 5$. While the intensity of this cumulative CO foreground is at least 2-100 times weaker than the current COBE/FIRAS upper limits, and has thus far evaded detection, it falls well above the detection limit of future instruments, such as PIXIE, which promise to measure CMB spectral distortions with sensitivity improved by 2-3 orders of magnitude compared to COBE/FIRAS.

In standard cosmology, there are a number of different heating/cooling processes in the early Universe which may have given rise to CMB spectral distortions of varying magnitudes and shapes. Silk damping of small-scale perturbations in the primordial baryon-electron-photon fluid is one of them, resulting in CMB distortions with magnitudes of $\Delta I_\nu / I_\nu \simeq 10^{-8} - 10^{-10}$, depending on the shape and amplitude of the primordial power spectrum at scales $50 \leq k \leq 10^4 \text{ Mpc}^{-1}$ (Daly 1991; Hu, Scott, & Silk 1994b; Chluba, Khatri, & Sunyaev 2012). Residual annihilation of dark matter particles throughout the history of the Universe is another, releasing energy that leads to μ and y distortions of amplitude $\mu \approx 3 \times 10^{-9}$ ($z > 5 \times 10^4$) and $y \approx 5 \times 10^{-10}$ ($z < 5 \times 10^4$), respectively (Chluba & Sunyaev

2012; Chluba & Jeong 2014). The cosmological recombination of hydrogen and helium is expected to have introduced distortions as well, with amplitudes of $\Delta I_\nu/I_\nu \simeq 10^{-9}$ at redshifts $z \sim 1100 - 6000$ (Chluba & Sunyaev 2006; Rubiño-Martín, Chluba, & Sunyaev 2006, 2008). Similar magnitude but opposite sign distortions, $\mu \sim -2.7 \times 10^{-9}$ and $y \sim -6 \times 10^{-10}$, are expected from energy losses of the CMB to baryons and electrons as they cool adiabatically faster than radiation with the expansion of the Universe (Chluba 2005; Chluba & Sunyaev 2012; Khatri, Sunyaev, & Chluba 2012).

Experiments like PIXIE will be able to constrain these spectral distortions in the CMB at the 5σ level, providing measurements at sensitivities $\mu = 5 \times 10^{-8}$ and $y = 10^{-8}$. However, as demonstrated above, the cumulative CO foreground is an important contaminant to these cosmological distortions, with a signal strength, $\Delta I_\nu^{\text{CO}}/I_\nu \sim 5 \times 10^{-6} - 10^{-7}$, that is 1-3 orders of magnitude higher than PIXIE's sensitivity limits in the frequency range $\nu \sim 20 - 360$ GHz. Based on the results depicted in Figure 2, CO luminous sources at redshifts $z < 8$ need to be identified and subtracted in order to reduce this cumulative signal to levels that are at least comparable to the μ - and y -type spectral distortions one hopes to constrain. Removing all such sources is challenging, both in terms of exposure time and in terms of field coverage. Even with ten hours of integration time, instruments like the Atacama Large Millimeter Array (ALMA) will miss CO emission from host halos with masses $M \lesssim 5 \times 10^{10} M_\odot$, which contribute tens of percent of the cumulative CO signal at redshifts $z \gtrsim 4$. (In this paper, we integrate over the population of CO luminous halos with masses $M \geq 10^{10} M_\odot$ and thus present conservative estimates of the total CO foreground which do not account for contributions from lower mass halos, $M \lesssim 10^{10} M_\odot$.) Removing the aggregate line emission from unresolved sources throughout cosmic history poses its own difficulties. Unlike the spectrally smooth synchrotron and thermal dust foregrounds which can be approximately described by power laws, the CO foreground fluctuates in frequency due to the clustering of sources over restricted regions on the sky; accurate foreground subtraction therefore requires knowledge of the emission spectrum to high order of precision, challenging our ability to fully exploit PIXIE's sensitivity to constrain CMB spectral measurements.

5 ACKNOWLEDGEMENTS

This research was also supported by the Raymond and Beverly Sackler Tel Aviv University - Harvard/ITC Astronomy Program. This work was supported in part by NSF grant AST-1312034. This material is based upon work supported by the National Science Foundation Graduate Research Fellowship under Grant No. DGE1144152. Any opinion, findings, and conclusions or recommendations expressed in this material are those of the authors and do not necessarily reflect the views of the National Science Foundation.

REFERENCES

André P., et al., 2014, JCAP, 2, 006

- Behroozi P. S., Wechsler R. H., Conroy C., 2013a, ApJ, 770, 57
 Behroozi P. S., Wechsler R. H., Conroy C., 2013b, ApJ, 762, L31
 Burigana C., Danese L., de Zotti G., 1991, A&A, 246, 49
 Burigana C., Salvaterra R., 2003, MNRAS, 342, 543
 Castor J. I., 1970, MNRAS, 149, 111
 Chluba, J., 2005, PhD thesis, Ludwig Maximilians University
 Chluba J., 2013, MNRAS, 436, 2232
 Chluba J., 2014, arXiv:1405.6938
 Chluba J., Sunyaev R. A., 2006, A&A, 458, L29
 Chluba J., Sunyaev R. A., 2012, MNRAS, 419, 1294
 Chluba J., Jeong D., 2014, MNRAS, 438, 2065
 Chluba J., Hamann J., Patil S. P., 2015, IJMPD, 24, 1530023
 Chluba J., Khatri R., Sunyaev R. A., 2012, MNRAS, 425, 1129
 Daly R. A., 1991, ApJ, 371, 14
 Danese L., de Zotti G., 1982, A&A, 107, 39
 Davies R., Mark, D., Sternberg, A., 2012, A&A, 537, 133
 Fixsen D. J., Cheng E. S., Gales J. M., Mather J. C., Shafer R. A., Wright E. L., 1996, ApJ, 473, 576
 Fixsen D. J., Dwek E., Mather J. C., Bennett C. L., Shafer R. A., 1998, ApJ, 508, 123
 Fixsen D. J., Mather J. C., 2002, ApJ, 581, 817
 Fixsen D. J., 2009, ApJ, 707, 916
 Goldreich P., Kwan J., 1974, ApJ, 189, 441
 Greve T. R., et al., 2014, ApJ, 794, 142
 Hill J. C., Battaglia N., Chluba J., Ferraro S., Schaan E., Spergel D. N., 2015, arXiv, arXiv:1507.01583
 Hu W., Silk J., 1993, PhRvD, 48, 485
 Hu W., Scott D., Silk J., 1994a, PhRvD, 49, 648
 Hu W., Scott D., Silk J., 1994b, ApJ, 430, L5
 Illarionov A. F., Sunyaev R. A., 1975a, SvA, 18, 413
 Illarionov A. F., Sunyaev R. A., 1975b, SvA, 18, 691
 Khatri R., Sunyaev R. A., Chluba J., 2012, A&A, 540, A124
 Kogut A., et al., 2011a, SPIE, 8146, 81460T
 Kogut A., et al., 2011b, JCAP, 7, 025
 Lutz D., 2014, ARA&A, 52, 373
 Mashian N., Sternberg A., Loeb A., 2015, JCAP, 11, 028
 Mashian N., Oesch P. A., Loeb A., 2016, MNRAS, 455, 2101
 Mather J. C., et al., 1994, ApJ, 420, 439
 Oh S. P., Cooray A., Kamionkowski M., 2003, MNRAS, 342, L20
 Planck Collaboration, et al., 2015, arXiv, arXiv:1502.01589
 Refregier A., Komatsu E., Spergel D. N., Pen U.-L., 2000, PhRvD, 61, 123001
 Righi M., Hernández-Monteagudo C., Sunyaev R. A., 2008, A&A, 489, 489
 Rubiño-Martín J. A., Chluba J., Sunyaev R. A., 2006, MNRAS, 371, 1939
 Rubiño-Martín J. A., Chluba J., Sunyaev R. A., 2008, A&A, 485, 377
 Sheth R. K., Tormen G., 1999, MNRAS, 308, 119
 Sunyaev R. A., Zeldovich Y. B., 1969, Natur, 223, 721
 Sunyaev R. A., Zeldovich Y. B., 1970, Ap&SS, 7, 20
 Sunyaev R. A., Khatri R., 2013, IJMPD, 22, 1330014
 Zeldovich Y. B., Sunyaev R. A., 1969, Ap&SS, 4, 301
 De Zotti G., Negrello M., Castex G., Lapi A., Bonato M., 2015, arXiv, arXiv:1512.04816